Synthesis and modelling of nanoparticles for chemical looping reforming

Stefan Andersson[1*], Paul Inge Dahl[1], Stephen A. Shevlin[2], Ingeborg-Helene Svenum[1], Yngve Larring[3], Julian R. Tolchard[1], Zheng Xiao Guo[2]

[1]*SINTEF Materials and Chemistry, P.O. Box 4760 Torgarden, 7465 Trondheim, Norway*
[2]*Department of Chemistry, University College London, Gower Street, London WC1E 6BT, United Kingdom*
[3]*SINTEF Materials and Chemistry, P.O. Box 124 Blindern, 0134 Oslo, Norway*

DOI: 10.5185/amlett.2018.1929
www.vbripress.com/aml

Abstract

Experimental and complementary modelling studies on the potential use of iron oxide nanoparticles in chemical looping reforming processes have been performed. In order to avoid coarsening of the nanoparticles, and thereby loss of reactivity, at relevant process temperatures (700-900°C), the active metal oxide was embedded in an inert support material of lanthanum silicate. Micro reactor tests indicate that partial combustion occurs in reactions of reduced iron oxide with methane instead of pure reforming. Density Functional Theory and kinetic Monte Carlo calculations have been used to support and complement the experiments. The modelling supports efficient reactivity towards exposure of hydrogen, which is also observed experimentally. Reactivity towards methane is only tested for the fully oxidized state, Fe_2O_3, and not for the reduced oxide, giving results that are complementary to the experiments.

Keywords: Chemical looping, nanoparticles, synthesis, modelling

Introduction

Chemical looping [**1**] is an emerging technology for producing electricity, fuels or chemicals with low CO_2 emissions. In Chemical Looping Combustion (CLC), dual fluidized beds are often used to circulate the solid oxygen carrier particles, which provide the oxygen for combustion in the fuel reactor. The reduction of the particles in the fuel reactor makes it necessary to circulate oxygen carriers to the other fluidized bed, the air reactor, where the particles are oxidized. Subsequently, they are circulated back to the fuel reactor for another combustion cycle, and so on. The separation of fuel from air has several positive features: the combustion process becomes simpler, the combustion efficiency is in principle higher than for standard power plants, NO_x emissions are significantly reduced since nitrogen is not present in the fuel reactor, and CLC generates a sequestration-ready CO_2 stream, after condensation of water vapor [**1**]. However, to achieve the necessary efficiency gains of CLC in practice, efficient oxygen carriers are crucial. Chemical Looping Reforming (CLR) [**1, 2**] techniques (see **Fig. 1**) follow the same basic outline as CLC, but here focus is on the catalytic production of CO and H_2, for use in chemical industry, or, in the latter case, as a clean fuel. The CLR process uses less air than CLC, such that only partial oxidation of the oxygen carrier particles is achieved. In CLR, CH_4 is reacted with a metal oxide in order to extract individual hydrogen atoms. Individual hydrogen atoms react together in order to form H_2, which then desorbs from the surface. In the process the metal oxide is reduced by the extraction of oxygen by reaction with carbon from methane, forming CO. A reduction sequence $Fe_2O_3 \rightarrow Fe_3O_4 \rightarrow FeO \rightarrow Fe$ is then expected. This work concentrates on the Fe-oxides hematite, Fe_2O_3, and magnetite, Fe_3O_4, which forms naturally when Fe_2O_3 is reduced. At elevated temperatures Chemical Looping Combustion might occur instead, where hydrogen and carbon are completely oxidized to form H_2O and CO_2. The aim of our study is to evaluate the suitability of the different iron oxides for CLR.

Kinetic studies of unsupported iron nanoparticles have revealed improved reactivity, reduced mass resistance and enhanced heat transfer [**3**]. However, at temperatures above 450°C, particle sintering results in coarsening of the particles (up to μm scale), and the observed benefits disappear. In order to utilize the nanostructured materials it is therefore necessary to endow them with much greater thermal stability. This can be achieved by dispersing the active nano-catalyst within an inert support material, which suppresses coarsening and sintering via physical separation [**4, 5**]. In effect, a "mechanical caging" mechanism stabilizes the nanoparticles in the mesopores of the support material [**6**]. Such stabilized nano-composites have been successfully synthesised through reverse emulsion processes [**7-8**], but these routes are neither cost efficient, environmentally friendly, nor viable for large-scale production. More cost effective and "green" synthesis routes are therefore sought within this work.

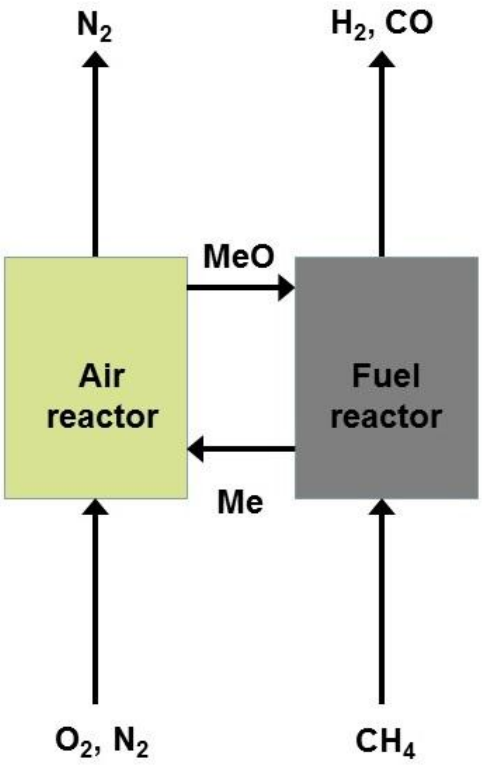

Fig. 1. Idealized schematic representation of complete CLR process, involving reduction of the metal oxide under methane to a less oxygen-rich phase. Syngas is outputted from this reactor. Meanwhile, the reduced material is reoxidized in a separate air reactor before being fed back into the fuel reactor.

The available literature on nanostructured oxygen carrier materials mostly considers first-row transition metals, which are then dispersed onto a thermally stabilizing amorphous barium hexaaluminate (BHA) support [**4, 5, 7, 9, 10**]. BHA as the support material has a high sintering temperature and low reactivity towards metal oxides under employed operating conditions. However, substitution of BHA due to cost and in some cases toxicity of Ba-precursors, is desirable. The current paper reports results obtained with the lanthanum silicate $La_{9.33}Si_6O_{26}$ as an alternative matrix material.

Modelling studies can be a highly valuable complement to experimental studies. Three different studies have recently been published using Density Functional Theory (DFT) to characterize mechanisms and reaction barriers of CH_4 reacting with a Fe_2O_3 surface [**11-13**]. Although the calculation setups are quite similar, the studies disagree both regarding detailed mechanisms, as well as the energetics of the individual reactions. The mechanism of initial dissociation of CH_4 into CH_3 and H is in all studies found to be occurring on top of a surface Fe atom with the product H atom adsorbed at a surface O site. Still, the calculated reaction barrier height varies between 1 and 2 eV. For this work, DFT calculations for this reaction were performed in order to clarify the important mechanisms as well as to form a basis for modelling the reaction kinetics.

In this paper we report on the synthesis, characterization and reactivity tests of nano-structured oxygen carrier particles as well as complementary modelling of the reactivity of iron oxide surfaces. In particular, we present kinetic Monte Carlo modelling results on the detailed kinetics of the CH_4 conversion to products as a function of temperature. This has to the best of our knowledge not been previously reported for chemical looping systems.

Experimental

Material synthesis

Active nanostructured particles embedded in an inert support were obtained by synthesis of a sol-gel of a composition which decomposes to two thermodynamically coexistent phases at high temperature. By forming the material as an atomically dispersed gel, the growth of the two phases can be controlled during gel heating/decomposition. Iron/iron oxide nanoparticles were embedded in a lanthanum silicate ($La_{9.33}Si_6O_{26}$) matrix in this fashion, via a modification of the method of Vojisavljević et.al. [**13**]. Lanthanum acetate, iron nitrate, ethanol and nitric acid are mixed with tetraethyl orthosilicate and heated to form a gel. This was then dried at 60 °C and heated at 230 °C to decompose into an amorphous powder. Upon further heat treatment a composite of lanthanum silicate and iron/iron oxide nanoparticles with a well defined loading (e.g., ~20 wt%) is obtained.

Characterization and reactivity tests

The synthesized materials were characterized by scanning electron microscopy (SEM) and X-ray diffraction (XRD). Furthermore, micro reactor tests were performed at 700-900ºC using 10% CH_4 + 3% H_2O in argon as the feed gas. Mass spectroscopy was applied to determine the concentrations of the gasses out of the reactor.

Computational details

A Density Functional Theory (DFT) approach was taken to model chemistry on metal oxide surfaces. The VASP code was used in all calculations [**15-18**], with a plane wave cutoff of 520 eV. The projector augmented wave (PAW) method was used to treat the core electrons [**19, 20**]. All atoms were fully relaxed until the change in force upon ionic displacement was less than 0.01 eV/Å, with the change in energies no greater than 10^{-5} eV. K-point meshes were chosen so that the difference in energies is less than 1 meV. The PBE+*U* functional is used in all calculations, with the *U* placed on the *d*-state of the Fe ions [**21**]. Literature studies of Fe-oxide materials use several different values for *U*, including 4.0 eV [**22-24**], 4.2 eV [**25**], and 5.0 eV [**26**]. We use a value of $U = 4.2$ eV as this gives a good match with experimental values. The Climbing Image Nudged Elastic Band method was used in order to determine the activation barriers for chemical reaction [**27**]. Four images were used in kinetics

calculations unless otherwise stated. As both metal oxides studied are magnetic, Fe_2O_3 being antiferromagnetic and Fe_3O_4 being ferromagnetic, spin-polarisation was used in all calculations. In this paper we only report on calculated results for Fe_2O_3. The corresponding results for Fe_3O_4 will be published in a future study.

The kinetic Monte Carlo (kMC) method [**28, 29**] was used to study the kinetics of the overall reactions occurring at the surface. For all calculations the kmos code was used [**30**]. Barrier heights derived from DFT calculations were used to calculate rate constants using simple Transition State Theory calculations [**28**]. The use of kMC allows for the kinetics of a system to be studied with greater accuracy than traditional microkinetic rate equation models. In particular, it allows for resolving a complex reactive system in *molecular detail* including individual sites and atoms and molecules. At the same time, there is no need to describe the system in *atomistic detail*, including molecular structures and interactions, such as for molecular dynamics or electronic structure calculations, allowing for fast simulations. In a *lattice kMC* model one only needs to specify a number of connected sites, populations of atoms and molecules at these sites, and the rates of reaction and transition (diffusion, adsorption, or desorption). Subsequently, a stochastic simulation of the motion and reaction of the species can be carried out, where one process at a time occurs.

Results and discussion

Characterization and reactivity tests

Electron microscopy characterization of the prepared materials is challenging due to the extremely small particle size, which limits the use of EDS elemental analysis. **Fig.** shows a sample which has been subjected to several reduction-oxidation cycles at 800 °C and 900 °C. The material shows quite unusual morphology, appearing "spotty". These spots are interpreted to be iron oxide particles of ~10-15 nm. This is supported by Rietveld analysis of XRD data (not presented here) which indicates iron oxide (Fe_3O_4) crystallites in the region of 22 nm. A similar sample redox-cycled at only 700 °C demonstrates a smaller crystallite size of around 12 nm.

Micro reactor tests up to 700°C show very little reforming of methane. Applying a pre-conditioning step by reducing the sample in humid hydrogen (10% H_2 + 3% H_2O in N_2) at 900°C for 20 minutes and subsequent reforming tests (10% CH_4 + 3% H_2O in Ar) at 900°C for 90 minutes gave interesting results, see **Fig. 1**. About 30% conversion of methane was found. However, a significant amount of CO_2 was produced indicating partial combustion. Mass 28 will have some contribution from N_2 background (one decade lower) and splitting of CO_2 in the MS which should be less than 0.3% in this case. Further tests are planned in order to obtain a better understanding of the results.

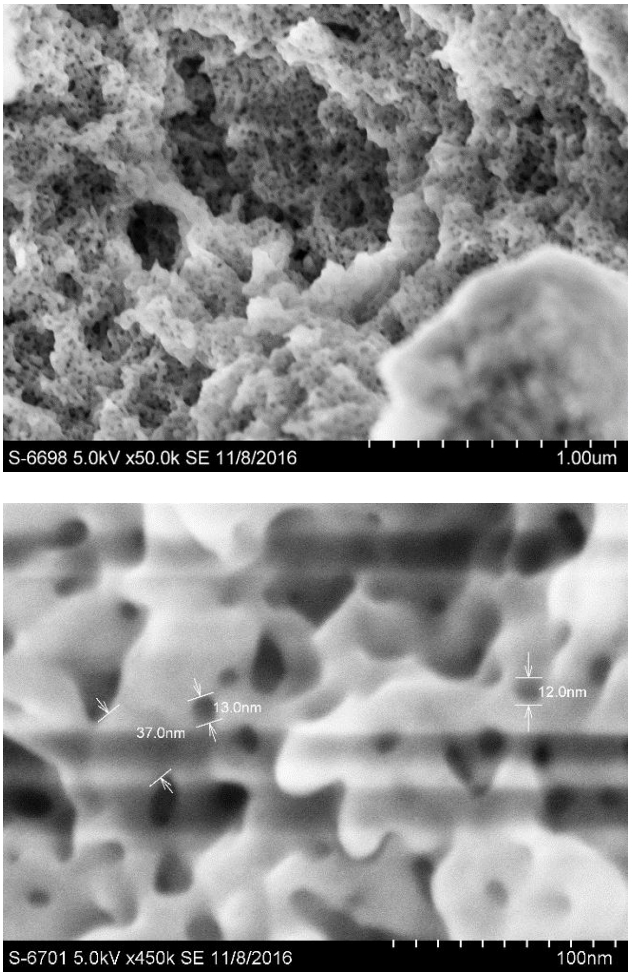

Fig. 2. Synthesized iron oxide nanoparticles on lanthanum silicate support.

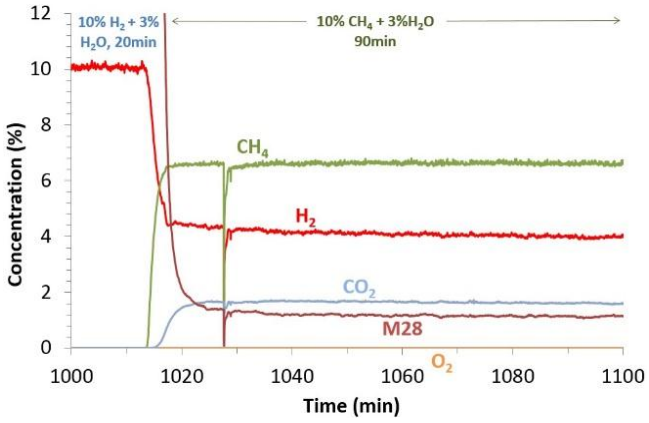

Fig. 1. Micro reactor reforming test at 900ºC with pre-conditioning of iron oxide nanoparticles on lanthanum silicate support.

Modelling

Fig. 4 shows the structures resulting from DFT calculations on CH_4 adsorption and dissociation on a Fe_2O_3 surface. The Fe-O_3-Fe surface termination was chosen since it has been found to be the most stable over a

wide range of oxygen pressures [**23**]. The CH_4 molecule is only weakly bound at a surface Fe site (**Fig. 4a)** with a binding energy of 0.16 eV. The barrier to dissociation of CH_4 into CH_3 and H, adsorbed at Fe and O sites (**Fig. 4b**), respectively, is 1.06 eV. As discussed earlier, literature values on this barrier height show a significant spread. In the DFT study by Huang et al. [**11**], whose results we have used for kinetic modelling (see below), this barrier is 1.76 eV. In addition, we find a reaction energy of 0.16 eV, whereas that of Huang et al. is 0.33 eV, but this is one of the smaller differences between this work and theirs. Another difference is that our calculations indicate that a solitary CH_3 species preferably binds to an O site **(Fig. 4c),** whereas Huang et al. conclude that CH_3 binds more strongly to a Fe site. The reasons for the above (and other) discrepancies between our work and the other DFT studies on this reaction [**11-13**] will need to be examined in more detail in the future.

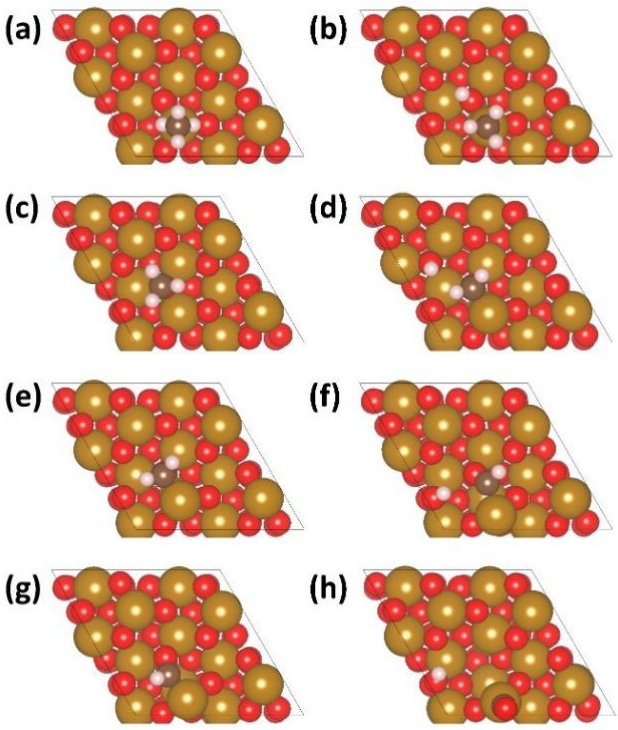

Fig. 4. Thermodynamically stable structures for CH_4 adsorption and molecular fragments produced upon reforming on the Fe_2O_3-(0001) surface. (a) is CH_4, (b) is CH_3+H, (c) is CH_3, (d) is CH_2+H, (e) is CH_2, (f) is CH+H, (g) is CH, and (h) is C+H. Iron is represented by large brown sphere, oxygen by small red sphere, carbon by small dark brown sphere, and hydrogen by small blue sphere.

In connection to the experiments on reduction of iron oxide by H_2 (**Fig. 3**), it is interesting to see that the DFT calculations predict a rather low barrier (0.4 eV) to H_2 dissociation at a surface Fe site. This barrier height is relative to H_2 in the gas phase, since H_2 adsorption to the Fe site is rather weak, with a binding energy of 0.18 eV. The coverage of adsorbed H_2 at 900°C is therefore expected to be extremely small. In contrast, the binding of a dissociated H_2 in the form of two H atoms at O sites is stable by 1.7 eV compared to gas-phase H_2. The reverse reaction has a barrier height of 2.1 eV to initiate H_2 formation from adsorbed H atoms. The energy required for two adsorbed H atoms to react with a surface O atom and desorb as a H_2O molecule is 1.8 eV, which effectively gives a lower activation energy than for H_2 formation. The conversion of H_2 into H_2O, and thereby reduction of the Fe_2O_3 surface, should therefore be a relatively efficient process, as the experimental results presented in **Fig. 3** suggest.

Finally, we report on kinetic Monte Carlo simulations using the whole set of elementary reaction steps as determined by DFT to evaluate the overall kinetics of CH_4 reacting with Fe_2O_3. Since the calculations by Huang et al. [**11**] are more extensive than ours and give qualitatively similar results where comparable, although the exact energetics differ in many cases (see above), we based the model on their results. We exchanged the initial barrier to CH_4 dissociation to our value (i.e., 1.76 eV to 1.06 eV) and derived the H atom diffusion barrier height between O sites from our results (0.49 eV). This constitutes Model A as given in **Table 1**. To further examine the effects of changing the individual rates we exchanged the mechanisms involving only adsorbed H atoms (e.g., H_2 and H_2O formation), from that of Huang et al. to our values (called Model B in **Table 1**). The surface O atom concentration was assumed to remain constant, meaning that replenishing O from the bulk when a surface O atom has reacted to form CO, CO_2, or H_2O is effectively instantaneous compared to the time scale of the reactions. From **Table 1** it can be seen that CO and H_2O should be the preferred products for the temperature range 700-1100°C, with only very minor production of CO_2. Experimentally, CO_2 production seemed to be comparable to and even exceeding CO production (**Fig. 3**). However, one should bear in mind that this was from a reduced iron oxide and simulations on Fe_3O_4 should therefore probably be better suited to compare to these experiments. This will form the topic of a future study.

Table 1. Branching fractions of CO and CO_2 products and H_2 and H_2O products from kMC simulations of CH_4 on Fe_2O_3.

	Model A		**Model A**		**Model B**	
T (°C)	X_{CO}	X_{CO2}	X_{H2}	X_{H2O}	X_{H2}	X_{H2O}
700	0.999	0.001	0.116	0.884	0.002	0.998
800	0.999	0.001	0.150	0.850	0.004	0.996
900	0.998	0.002	0.183	0.817	0.006	0.994
1000	0.997	0.003	0.213	0.787	0.008	0.992
1100	0.994	0.006	0.241	0.759	0.011	0.989

Conclusion

We have reported results on both experimental (synthesis, characterization, and reactivity tests) and modelling studies of iron oxide nanoparticles for the potential use in chemical looping reforming processes. Nanoparticles of iron oxide of size <20 nm were successfully embedded in an inert support (lanthanum silicate) via a simple, scalable and relatively cheap synthesis route and shown to be stable to temperatures appropriate for chemical looping processes. Micro reactor tests on the reactivity were carried out. By exposure to humid hydrogen, the iron oxide nanoparticles were reduced. Further tests of the reactivity of reduced iron oxide with CH_4 indicated that both CO and CO_2 were formed as significant products at 900°C, meaning that partial combustion occurs, instead of pure reforming where mainly CO (and H_2) should be formed. Further tests are needed to investigate whether the capabilities for reforming can be enhanced. DFT calculations on the reaction mechanisms and energetics of H_2 reacting with a fully oxidized Fe_2O_3 surface confirm that H_2O formation, and thereby reduction of the oxide, should be efficient. Kinetic Monte Carlo simulations of CH_4 reacting with Fe_2O_3, based on DFT calculations, indicate that CO and H_2O should be the dominating products in this case. Simulations on a reduced oxide surface, Fe_3O_4, will be the topic of a future study. Then both the effects on reactivity of reducing the oxide as well as the predictive power of the modelling can be properly assessed in comparing to experiments.

Acknowledgements

We acknowledge funding by a European Union FP7 grant: NanoSim – A Multiscale Simulation-Based Design Platform for Cost-Effective CO_2 Capture Processes using Nano-Structured Materials (project number 604656).

Author's contributions

Conceived the plan: PID, SA, SAS; Performed the experiments: JRT, PID, YL; Performed the modelling: SAS, IHS, SA; Wrote the paper: SA, PID, SAS, JRT, IHS, YL. Authors have no competing financial interests.

References

1. Adanez, J.; Abad, A.; Garcia-Labiano, F.; Gayan, P.; *Prog. Energ. Combust. Sci.*, **2012**, *38*, 215. **DOI:** 10.1016/j.pecs.2011.09.001
2. Rydén, M.; Lyngfelt, A.; Mattisson, T.; *Energy Fuels*, **2008**, *22*, 2585. **DOI:** 10.1021/ef800065m
3. Wen, D.; Song, P.; Zhang, K.; Qian, J.; *J. Chem. Technol. Biotechnol.*, **2011**, *86*, 375. **DOI:** 10.1002/jctb.2526
4. Kirchhoff, M.; Specht, U.; Veser, G. Synthesis and characterization of high temperature stable nanocomposite catalysts, In NSTI-Nanotech 2004, Vol 3, Technical Proceedings; Laudon, M.; Romanowicz, B. (Eds.); **2004**, pp. 268-271. http://www.nsti.org/publications/Nanotech/2004/pdf/B3-72.pdf
5. Kirchhoff, M.; Specht, U.; Veser, G.; *Nanotechnology*, **2005**, *16*, S401. **DOI:** 10.1088/0957-4484/16/7/014
6. Veser, G.; *Catal. Today*, **2010**, *157*, 24. **DOI:** 10.1016/j.cattod.2010.04.040
7. Solunke, R. D.; Veser, G.; *Energy Fuels*, **2009**, *23*, 4787. **DOI:** 10.1021/ef900280m
8. Bhavsar, S.; Najera, M.; Veser, G.; *Chem. Eng Technol.*, **2012**, *35*, 1281. **DOI:** 10.1002/ceat.201100649
9. Zarur, A. J.; Ying, J. Y.; *Nature*, **2000**, *403*, 65. **DOI:** 10.1038/47450
10. Zarur, A. J.; Hwu, H. H.; Ying, J. Y.; *Langmuir*, **2000**, *16*, 3042. **DOI:** 10.1021/la9908034
11. Huang, L.; Tang, M.; Fan, M.; Cheng, H.; *Appl. Ene.*, **2015**, *159*, 132. **DOI:** 10.1016/j.apenergy.2015.08.118
12. Tang, J.-J., and Liu, B; *J. Phys. Chem. C*, **2016**, *120*, 6642. **DOI:** 10.1021/acs.jpcc.6b00374
13. Cheng, Z.; Qin, L.; Guo, M.; Xu, M.; Fan, J. A.; Fan, L.-S.; *Phys. Chem. Chem. Phys.*, **2016**, *18*, 32418. **DOI:** 10.1039/c6cp06264d
14. Alsuhaim, H.S.; Vojisavljevic, V.; Pirogova, E.; *J. Elecromagn. Waves. Appl.*, **2014**, *28*, 1726. **DOI:** 10.1080/09205071.2014.934924
15. Kresse, G.; Hafner, J.; *Phys. Rev. B*, **1993**, *47*, R558. **DOI:** 10.1103/PhysRevB.47.558
16. Kresse, G.; Hafner, J.; *Phys. Rev. B*, **1994**, *49*, 14251. **DOI:** 10.1103/PhysRevB.49.14251
17. Kresse, G.; Furthmüller, J.; *Comput. Mater. Sci.*, **1996**, *6*, 15. **DOI:** 10.1016/0927-0256(96)00008-0
18. Kresse, G.; Furthmüller, J.; *Phys. Rev. B*, **1996**, *54*, 11169. **DOI:** 10.1103/PhysRevB.54.11169
19. Blöchl, P. E..; *Phys. Rev. B*, **1996**, *50*, 17953. **DOI:** 10.1103/PhysRevB.50.17953
20. Kresse, G.; Joubert, D.; *Phys. Rev. B*, **1999**, *59*, 1758. **DOI:** 10.1103/PhysRevB.59.1758
21. Dudarev, S. L.; Botton, G. A.; Savrasov, S. Y.; Humphreys, C. J.; Sutton, A. P.; *Phys. Rev. B*, **1998**, *57*, 1505. **DOI:** 10.1103/PhysRevB.57.1505
22. Souvi, S. M. O.; Badawi, M.; Paul, J.-F.; Cristol, S.; Cantrel, L.; *Surf. Sci.*, **2013**, *610*, 7. **DOI:** 10.1016/j.susc.2012.12.012
23. Kiejna, A.; Pabisiak, T.; *J. Phys.: Condens. Mat.*, **2012**, *24*, 095003. **DOI:** 10.1088/0953-8984/24/9/095003
24. Rollmann, G.; Rohrbach, A.; Entel, P.; Hafner, J.; *Phys. Rev. B*, **2004**, *69*, 165107. **DOI:** 10.1103/PhysRevB.69.165107
25. Nguyen, M.-T.; Seriani, N.; Piccinin, S.; Gebauer, R.; *J. Chem. Phys.*, **2014**, *140*, 064703. **DOI:** 10.1063/1.4865103
26. Ling, L.; Song, J.; Zhao, S.; Zhang, R.; Wang, B.; *RSC Adv.*, **2014**, *4*, 22411. **DOI:** 10.1039/C4RA02485K
27. Henkelman, G.; Jónsson, H.; *J. Chem. Phys.*, **2000**, *113*, 9901. **DOI:** 10.1063/1.1329672
28. Jansen, A. P. J.; An Introduction to Kinetic Monte Carlo Simulations of Surface Reactions; Springer, **2012**. **DOI:** 10.1007/978-3-642-29488-4
29. Reuter, K.; Scheffler, M.; *Phys. Rev. B*, **2006**, *73*, 045433. **DOI:** 10.1103/PhysRevB.73.045433
30. Hoffmann, M. J.; Matera, S.; Reuter, K.; *Computer Phys. Commun.*, **2014**, *185*, 2138. **DOI:** 10.1016/j.cpc.2014.04.003

